Ternary fission of a heavy nuclear system within a three-center shell model

A. V. Karpov*
Flerov Laboratory of Nuclear Reactions, JINR, 141980 Dubna, Russia
and Dubna State University, 141986 Dubna, Russia
(Received 10 October 2016; published 27 December 2016)

Background: Since more than 40 years of theoretical and experimental studies of true ternary fission, one is still quite far from its understanding. The true ternary fission channel, being strongly suppressed by the macroscopic properties of the potential energy, may, however, be present with a significant probability due to shell effects.
Purpose: Development of a model for the multidimensional potential energy suitable for analysis of the nucleus-nucleus collisions with the possibility of ternary exit channel. Study of the potential possibility of fission of actinides into three heavy fragments.
Method: The asymmetric three-center shell model of deformed nucleus is developed in this paper. The model can be applied for analysis of ternary as well as binary fission processes.
Results: The potential energy surfaces for few ternary combinations in the fission channel are calculated for the ^{252}Cf nucleus. Their properties are discussed.
Conclusions: The potential energy structures are compared with the experimental observations. It was found that the potential energy has pronounced valleys favorable for ternary fission with formation of doubly magic tin as one of the fragments and two other lighter fragments. The positions of the found fission valleys are in a good agreement with the experimental data.

DOI: 10.1103/PhysRevC.94.064615

I. MOTIVATION

In spite of the fact that a lot of studies of the fission process have been performed since its discovery in 1938, fission physics still has exciting topics to be explored and understood. One of them is the process of ternary fission. Here one should distinguish between two different processes, namely "ternary fission" and "true ternary fission." Ternary fission is the process of formation of a light charged particle (mainly, an α particle) accompanying fission and emitted with the largest probability in the perpendicular direction to the fission axis. The probability of this process decreases exponentially with the increase of the fragment mass. This supports the idea that the third fragment appears as a fluctuation in the neck region. Nearly complete information on this process can be found in Refs. [1–3] (see also Refs. [4,5] for recent experimental studies).

The term "true ternary fission" is used for a simultaneous decay of a heavy nucleus into three fragments of comparable masses [1]. True ternary fission is considered as a process similar to the binary fission connected with a large-scale evolution of the nuclear shape from the compact configuration of the initial nucleus through formation of two necks and final division of a composite system into three fragments.

True ternary fission of atomic nuclei (below the word "true" is omitted) has a long history of theoretical and experimental studies. Early theoretical considerations based on the liquid drop model (LDM) [6] showed that, for heavy nuclei, ternary fission produces a larger total energy release in comparison to binary fission, but the actual possibility of ternary fission is determined, in fact, not by the total energy release but by the barrier properties. It was found that the LDM ternary fission barriers for oblate (triangular) deformations are much higher compared to the barriers of prolate configurations [7], and it seems that the oblate ternary fission may be excluded from consideration. However, further study of this problem within the more sophisticated three-center shell model [8] showed that the shell effects may significantly reduce the ternary fission barriers even for oblate deformations of very heavy nuclei. Recently [9] the potential energy as well as the tunneling probability were calculated within the three-center shell model for the isotopes of element 120. The calculations were performed assuming equal masses of all three fragments (division into three zirconium isotopes). The authors conclude that such a process is very improbable due to the high fission barrier. Another extensive study of the true ternary fission of ^{252}Cf was performed recently in Refs. [10–12] based on the consideration of the potential energy surface at contact configuration of three preformed clusters. These studies have confirmed, in particular, the preference of the collinear configuration of three fragments over the triangular one.

The experimental information on the true ternary fission is rather limited. Study of this process performed by M. L. Muga with colleagues [13] for spontaneous fission of ^{252}Cf and thermal neutron-induced fission of few uranium isotopes has showed that the ratio of ternary events to the binary ones is about 10^{-6}. Another investigation of symmetric ternary spontaneous fission of ^{252}Cf was done by Schall *et al.* [14]. The deduced upper limit for the symmetric ternary to binary fission ratio is 10^{-8} s. The extensive search for the ternary decay channel was performed by the group of D. Kamanin (see Ref. [15] and references therein) for the spontaneous fission of ^{252}Cf as well as for thermal neutron-induced fission of ^{235}U. The searched for process was named "collinear cluster tri-partition" since the decay products fly apart almost collinearly. It was found that the true ternary fission is a rather probable channel with the yield ratio to the binary one of about 10^{-4}. The increased ternary yield is detected in the

*karpov@jinr.ru

spontaneous fission of ^{252}Cf for the following combinations with formation of magic or semimagic clusters: Sn+Ge(or Ni)+S(or Ca). Another dedicated experiment has shown that the ternary fission with formation of ^{68}Ni or ^{72}Ni as one of the fragments has an increased yield as well.

Today it becomes possible to study experimentally the properties and dynamics of the formation and decay of superheavy nuclei, for which true ternary fission could be rather probable. It is well known that for superheavy nuclei the LDM fission barriers are rather low (or vanish) and the shell correction to the total deformation energy is very important. First estimations of the binary and prolate ternary fission barriers of the superheavy nucleus ^{298}114, made in Ref. [16] with the approximately calculated shell corrections, demonstrated their closeness within 10%. This result was later confirmed in Ref. [17] within the temperature-dependent LDM. The possibility of symmetric true ternary fission and quasifission (with equal outer fragments) was considered recently in Ref. [18] based on the potential energy calculations. It was found that the ternary fission is quite possible for superheavy nuclei, and it is connected with three-body clusterization with the formation of two tinlike fragments and a heavy third fragment in between. For example, in the case of the ^{64}Ni+^{238}U reaction, one may expect the ternary exit channel like ^{132}Sn+^{38}Ca+^{132}Sn with three magic nuclides as the fragments. Even larger shell effects are predicted for the giant nuclear systems formed in collisions of actinides. Here the fusion-fission process is not possible at all; however, the ternary quasifission in U+U collisions with the formation of two leadlike outer fragments is extremely favorable. Note that it is sufficient to detect two coincident leadlike ejectiles (or one leadlike and one calcium-like fragments) in U+U collisions to unambiguously prove the existence of ternary quasifission of a giant nuclear system. Such experiments are under discussion for the near future.

The present work is aimed at the development of a model for the multidimensional potential energy suitable for the modeling of nucleus-nucleus collisions (binary entrance channel) with the possibility to have two as well as three fragments in the exit channel. The potential energy model should provide (i) a rich-enough nuclear shape parametrization giving realistic entrance-channel shapes (rather compact contact configuration) as well as elongated scission shapes with pronounced necking; (ii) a smooth variation of nuclear shapes with the growing third fragment (the middle one), including a smooth transition from the binary to ternary fission shapes; and (iii) a correct description of the fusion barriers in the entrance channel as well as ground-state properties and fission barriers. Another purpose of the paper is to test the model on the existing experimental data on the true ternary fission. That is possible since all the features seen in the experiment (such as increased yields for a certain combination of fragment masses) should be present in the potential energy landscape as well.

II. THREE-CENTER SHELL MODEL

The macro-microscopical approach is used as a standard method of calculation of the potential energy of a deformed nuclear system. Within the macro-microscopic approach, the potential energy is usually composed of two parts, $V_{\rm mac-mic}(A,Z;{\rm shape}) = V_{\rm mac}(A,Z;{\rm shape}) + \delta E(A,Z;{\rm shape})$. The macroscopic part, $V_{\rm mac}$, smoothly depends on the proton and neutron numbers and may be calculated within the liquid-drop model. In particular, in this work, the finite-range liquid-drop model (see, e.g., Ref. [19]) with the parameters determined in Ref. [20] is used. The microscopic part, δE, describes the shell effects. It is constructed from the single-particle energy spectra by the Strutinsky procedure [21]. The single-particle states required for the shell correction calculation can be obtained by diagonalization of the Hamiltonian of a model on the basis of the chosen wave functions. The problem is significantly simplified if all of the matrix elements can be calculated analytically. This can be achieved by the proper choice of the mean-field potential and basis functions.

One of the most successful models of such kind giving the single-particle spectrum of a deformed binary nuclear system is the two-center shell model (TCSM). The model was first proposed in Ref. [22] and later on developed by the Frankfurt group [23–25]. In spite of the fact that the standard two-center shell model works well for the ground-state and saddle-point deformations, it (being applied to the whole system) fails in the region of the Coulomb barrier in the entrance channel of the fusion reaction and also in the region of two well-separated nuclei [20,26,27]. The standard model cannot describe correctly the transition from the potential energy of a mononucleus to the potential energy of separated nuclei. An extended macro-microscopic approach was proposed in Ref. [20] for the simultaneous analysis of deep-inelastic collisions, quasifission, and fusion-fission processes. The mentioned problem of the standard model was solved within this model. The idea was to use the correct properties of the standard macro-microscopical approach for compact nuclear shapes and moderate deformations (typical for fission saddle points), while the potential energy (or mass) of the system at extreme deformations of scission point (or Coulomb barrier) as well as for separated nuclei can be easily calculated as a sum of the interaction potential (e.g., folding)

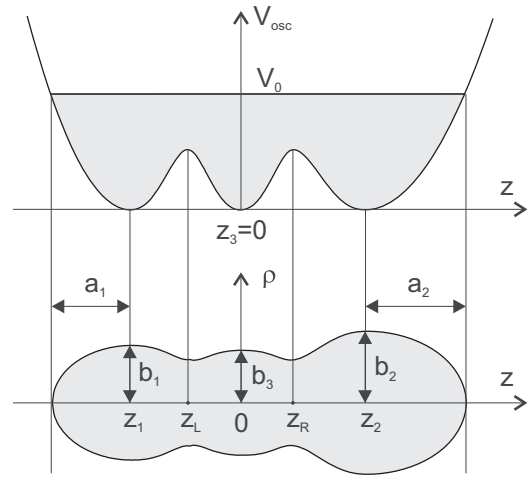

FIG. 1. Example of the three-center shell model potential $V_{\rm osc}$ (top) and the corresponding nuclear shape (bottom).

and two deformation energies of the fragments. In between a smooth transition between these two cases is used.

In the following, the key relations of the developed three-center shell model (T3CSM) are given. The T3CSM is developed in a similar way as the TCSM. The basic constituent of the macro-microscopical model is the shape parametrization that depends on a set of chosen collective degrees of freedom. An axial symmetric nuclear shape in the T3CSM is obtained by three smoothly joined ellipsoids with semiaxes a_i and b_i ($i = 1,2,3$). The Hamiltonian of the model is

$$\hat{H} = -\frac{\hbar^2}{2m_0}\nabla^2 + V_{\rm osc}(\vec{r}) + V_{\rm LS}(\vec{r},\vec{p},\vec{s}) + V_{L^2}(\vec{r},\vec{l}). \quad (1)$$

Denoting the positions of the three centers by z_1, z_2 (side fragments), and z_3 (middle fragment), the momentum independent part of the potential in cylindrical coordinates $\{z,\rho,\phi\}$ (independent of ϕ due to the system axial symmetry) may be expressed as

$$V_{\rm osc}(\rho,z) = \frac{1}{2}\,m_0 \begin{cases} \omega_{z1}^2\,(z-z_1)^2 + \omega_{\rho 1}^2\,\rho^2; & z \leqslant z_1; \\ \omega_{z1}^2\,(z-z_1)^2\,[1 + c_1(z-z_1) + d_1(z-z_1)^2] + \omega_{\rho 1}^2\,[1 + g_1(z-z_1)^2]\rho^2; & z_1 < z \leqslant z_L; \\ \omega_{z3}^2\,(z-z_3)^2\,[1 + c_3(z-z_3) + d_3(z-z_3)^2] + \omega_{\rho 3}^2\,[1 + g_{31}(z-z_3)^2]\rho^2; & z_L < z \leqslant z_3; \\ \omega_{z3}^2\,(z-z_3)^2\,[1 - c_3(z-z_3) + d_3(z-z_3)^2] + \omega_{\rho 3}^2\,[1 + g_{32}(z-z_3)^2]\rho^2; & z_3 < z \leqslant z_R; \\ \omega_{z2}^2\,(z-z_2)^2\,[1 + c_2(z-z_2) + d_2(z-z_2)^2] + \omega_{\rho 2}^2\,[1 + g_2(z-z_2)^2]\rho^2; & z_R < z \leqslant z_2; \\ \omega_{z2}^2\,(z-z_2)^2 + \omega_{\rho 2}^2\,\rho^2; & z > z_2. \end{cases} \quad (2)$$

Here m_0 is the nucleon mass, and ω_{zi} and $\omega_{\rho i}$ are the frequencies of the oscillators defined along the symmetry axis and perpendicular to it. They are connected with the semiaxes as

$$a_i = R_0\omega_0/\omega_{zi}, \quad b_i = R_0\omega_0/\omega_{\rho i}, \qquad R_0 = r_0 A^{1/3}, \quad \hbar\omega_0 = 41/A^{1/3}\ \text{MeV}, \quad (3)$$

where $r_0 = 1.16$ fm is the nuclear radius parameter and A is the nucleus mass number. An example of the T3CSM mean-field potential along with the corresponding nuclear shape is shown in Fig. 1. The shape profile function has local maxima (while the potential has minima) at the positions of the oscillator centers z_1, z_2, and $z_3 = 0$. Similarly, the z_L and z_R values correspond to the minima of the shape profile (maxima of the potential). The thicknesses of the shape at z_L and z_R are assumed to be equal, which leads to simultaneous rupture of both necks at the moment of ternary scission.

The momentum-dependent part of the potential consists of a spin-orbit coupling term

$$V_{\rm LS}(\vec{r},\vec{p},\vec{s}) = \begin{cases} \left\{ -\frac{\hbar\kappa_1}{m_0\,\omega_{01}}, (\nabla V_{\rm osc} \times \vec{p})\cdot\vec{s} \right\}; & z \leqslant z_L; \\ \left\{ -\frac{\hbar\kappa_3}{m_0\,\omega_{03}}, (\nabla V_{\rm osc} \times \vec{p})\cdot\vec{s} \right\}; & z_L < z \leqslant z_R; \\ \left\{ -\frac{\hbar\kappa_2}{m_0\,\omega_{02}}, (\nabla V_{\rm osc} \times \vec{p})\cdot\vec{s} \right\}; & z > z_R \end{cases} \quad (4)$$

and an l^2-like term

$$V_{L^2}(\vec{r},\vec{l}) = \frac{1}{2} \begin{cases} -\left\{ \frac{\hbar\kappa_1}{m_0^2\,\omega_{01}^3}, l^2 \right\} + \hbar\omega_{01}\,\kappa_1\,\mu_1\,N_1(N_1+3)\delta_{if}; & z \leqslant z_L; \\ -\left\{ \frac{\hbar\kappa_3}{m_0^2\,\omega_{03}^3}, l^2 \right\} + \hbar\omega_{03}\,\kappa_3\,\mu_3\,N_3(N_3+3)\delta_{if}; & z_L < z \leqslant z_R; \\ -\left\{ \frac{\hbar\kappa_2}{m_0^2\,\omega_{02}^3}, l^2 \right\} + \hbar\omega_{02}\,\kappa_2\,\mu_2\,N_2(N_2+3)\delta_{if}; & z > z_R. \end{cases} \quad (5)$$

In these formulas $\{A,B\} = A\,B + B\,A$ denotes the anti-commutator of two quantities and δ_{if} is a purely diagonal operator; κ_i is the spin-orbit interaction constant; μ_i is the adjustable parameter of the Nilsson model; N_i is the oscillator shell number for the side or middle part of the nucleus; and $\hbar\omega_{0i} = 41/\tilde{A}_i$ MeV is the energy level spacing of the spherical oscillator, where $\tilde{A}_i$ is the asymptotic mass number of the nuclear fragment, which is defined in Ref. [25] as $\tilde{A}_i = a_i b_i^2/r_0^3$. The parameters N_i and $\tilde{A}_i$ are determined in such a way that for the elliptic shape of the initial nucleus, they should be the oscillator shell number and the nuclear mass number, while for the asymptotic state of separated nuclei they are the corresponding values for the fragments.

The nuclear shape is determined by the profile function $\rho_s(z)$ and can be obtained by assigning $V_{\rm osc}(\rho_s,z) = V_0$, where $V_0 = 1/2 m_0\omega_0 R_0^2$ (see Fig. 1). It is clear that the parts of the shape, external with respect to z_1 and z_2, are axially symmetric ellipsoids centered at z_i with semiaxes a_i and b_i ($i = 1,2$). The internal part of the shape is more complicated. The shape parametrization (as well as the mean-field potential $V_{\rm osc}$) has 21 free parameters: z_i, a_i, b_i, c_i, d_i ($i = 1,2,3$), g_1, g_2, g_{31}, g_{32}, z_L, and z_R. It is assumed that $z_3 = 0$. Another 13 parameters can be fixed in the same way as done in Ref. [25], imposing the conditions of volume conservation and the continuity of the parametrization and its first derivative at the matching points z_L and z_R. Therefore, the shape parametrization of the T3CSM

has seven independent parameters that allows one to introduce seven collective variables: the elongation of the system $R = z_2 - z_1$, which for separated fragments is approximately the distance between the mass centers of the side fragments; the ellipsoidal deformations of the three parts of the system, $\delta_i = a_i/b_i - 1$; two mass-asymmetry parameters $\eta_{21} = (A_2 - A_1)/(A_2 + A_1)$ and $\eta_3 = A_3/(A_1 + A_2 + A_3)$, where A_1, A_2, and A_3 are the mass numbers of the fragments; and the neck parameter ϵ. This parameter arises due to the smoothing of the potential $V_{\rm osc}(\rho,z)$ in the region between the oscillator centers and is defined as the ratio of the smoothed and pure harmonic oscillator potentials at the crossing point of the harmonic oscillator potentials z_L and z_R (see, e.g., Fig. 9 of Ref. [20]). Therefore, smaller values of ϵ correspond to a thicker neck at fixed values of the other parameters.

The basic functions required for the diagonalization of the Hamiltonian (1) are the solutions of the three-center problem,

$$\hat{H}_0\psi = E_0\psi, \quad \hat{H}_0 = -\frac{\hbar^2}{2m_0}\nabla^2 + V_{\rm osc}(\rho,z), \tag{6}$$

where the mean-field potential is taken without smoothing ($c_i = d_i = g_i = 0$). The corresponding Schrödinger equation for the pure three oscillator potentials (6) is separable when $\omega_{\rho_1} = \omega_{\rho_2} = \omega_{\rho_3} \equiv \omega_\rho$. When solved, this equation produces the basis for further calculation within the T3CSM. The total single-particle wave function reads

$$\psi(\rho,z,\phi) = \Phi_{n_z}(z)\chi^{|m|}_{n_\rho}(\rho)\eta_m(\phi), \tag{7}$$

where

$$\eta_m(\phi) = \frac{1}{\sqrt{2\pi}}\exp(im\phi), \tag{8}$$

$$\chi^{|m|}_{n_\rho}(\rho) = N_\rho^{-1}\, k_\rho^{\frac{|m|+1}{2}}\, \exp\left(-\frac{k_\rho\,\rho^2}{2}\right)\rho^{|m|}\, L^{|m|}_{n_\rho}(k_\rho\,\rho^2) \tag{9}$$

with the normalization constant N_ρ and $k_\rho = \frac{m_0\,\omega}{\hbar}$, n_ρ is a non-negative integer, and $L^\alpha_n(x)$ is the Laguerre polynomial.

The z-dependent function Φ_{n_z} is defined in three regions corresponding to the three nascent fragments

$$\Phi_{n_z}(z) = \begin{cases} N_{z_1}^{-1}\, U\big(-n_{z_1} - \frac{1}{2}, -\sqrt{2k_{z_1}}\,(z - z_1)\big), & z \leqslant z_L; \\ N_{z_{3U}}^{-1}\, U\big(-n_{z_3} - \frac{1}{2}, \sqrt{2k_{z_3}}\,(z - z_3)\big) + N_{z_{3V}}^{-1}\, V\big(-n_{z_3} - \frac{1}{2}, \sqrt{2k_{z_3}}\,(z - z_3)\big), & z_L < z \leqslant z_R; \\ N_{z_2}^{-1}\, U\big(-n_{z_2} - \frac{1}{2}, \sqrt{2k_{z_2}}\,(z - z_2)\big), & z > z_R \end{cases} \tag{10}$$

with the normalization factors N_{z_1}, N_{z_2}, N_{z_3U}, and N_{z_3V}. Here $U(a,x)$ and $V(a,x)$ are the regular and irregular parabolic cylinder functions defined by

$$U(a,x) = \sqrt{\pi}\, 2^{-\frac{1}{2}a-\frac{1}{4}} e^{-\frac{x^2}{4}} \frac{{}_1F_1\big(\frac{1}{2}a + \frac{1}{4}; \frac{1}{2}; \frac{1}{2}x^2\big)}{\Gamma\big(\frac{1}{2}a + \frac{3}{4}\big)} - x\,\sqrt{\pi}\, 2^{-\frac{1}{2}a+\frac{1}{4}} e^{-\frac{x^2}{4}} \frac{{}_1F_1\big(\frac{1}{2}a + \frac{3}{4}; \frac{3}{2}; \frac{1}{2}x^2\big)}{\Gamma\big(\frac{1}{2}a + \frac{1}{4}\big)} \tag{11}$$

and

$$V(a,x) = \sqrt{\pi}\, 2^{-\frac{1}{2}a-\frac{1}{4}} \tan\left[\pi\left(\frac{1}{4} + \frac{1}{2}a\right)\right] \times \frac{{}_1F_1\big(\frac{1}{2}a + \frac{1}{4}; \frac{1}{2}; \frac{1}{2}x^2\big)e^{-\frac{x^2}{4}}}{\Gamma\big(\frac{1}{2}a + \frac{3}{4}\big)\Gamma\big(\frac{1}{2} - a\big)} - x\,\sqrt{\pi}\, 2^{-\frac{1}{2}a+\frac{1}{4}} \tan^{-1}\left[\pi\left(\frac{1}{4} + \frac{1}{2}a\right)\right] \times \frac{{}_1F_1\big(\frac{1}{2}a + \frac{3}{4}; \frac{3}{2}; \frac{1}{2}x^2\big)e^{-\frac{x^2}{4}}}{\Gamma\big(\frac{1}{2}a + \frac{1}{4}\big)\Gamma\big(\frac{1}{2} - a\big)}, \tag{12}$$

whose properties may be found in Ref. [28]. The seven n_{zi} and N_{zi} coefficients entering Eq. (10) can be determined numerically in a standard way by imposing the normalization condition and the condition of smoothness of the wave function and its first derivative at the matching points

$$\int_{-\infty}^{\infty}\Phi_{n_z}(z)dz = 1,$$

$$\Phi_{n_{z1}}(z_L) = \Phi_{n_{z3}}(z_L), \quad \Phi_{n_{z2}}(z_R) = \Phi_{n_{z3}}(z_R),$$

$$\Phi'_{n_{z1}}(z_L) = \Phi'_{n_{z3}}(z_L), \quad \Phi'_{n_{z2}}(z_R) = \Phi'_{n_{z3}}(z_R),$$

$$\omega_{z_1}\left(n_{z_1} + \frac{1}{2}\right) = \omega_{z_2}\left(n_{z_2} + \frac{1}{2}\right) = \omega_{z_3}\left(n_{z_3} + \frac{1}{2}\right). \tag{13}$$

The last equation in Eq. (13) ensures that the eigenvalue $E_0 = \hbar\omega_{zi}(n_{zi} + 1/2) + \hbar\omega_\rho(2n_\rho + 1)$ is independent of the space coordinates.

Finally, the eigenvalues and eigenvectors of the initial problem (1) are found by the standard diagonalization procedure with the cut-off energy for the basis functions equal to $12\hbar\omega_0$.

III. RESULTS AND DISCUSSION

There are too many collective degrees of freedom necessary for proper description of the potential energy of a nuclear configuration consisting of three deformed heavy fragments. As mentioned above, the three-center parametrization has seven degrees of freedom. The number of collective variables has been restricted in order to test the developed model. Instead of three independent deformation parameters δ_i, I use a single unified deformation δ_U defined in the same way as in Ref. [20],

$$3\delta_U = (\delta_1 - \tilde{\delta}_1) + (\delta_2 - \tilde{\delta}_2) + (\delta_3 - \tilde{\delta}_3),$$
$$C_{\delta 1}(\delta_1 - \tilde{\delta}_1) = C_{\delta 2}(\delta_2 - \tilde{\delta}_2) = C_{\delta 3}(\delta_3 - \tilde{\delta}_3), \tag{14}$$

where $\tilde{\delta}_i$ are the deformation parameters providing the minimum of the potential energy for the fixed other collective variables. The second relation in Eq. (14) is, in fact, the balance equation of forces applied to three deformed nuclear fragments. Equation (14) is limited to second-order terms in the expansion of deformation energies into series in the deformation. The rigidity parameters $C_{\delta i}$ can be evaluated

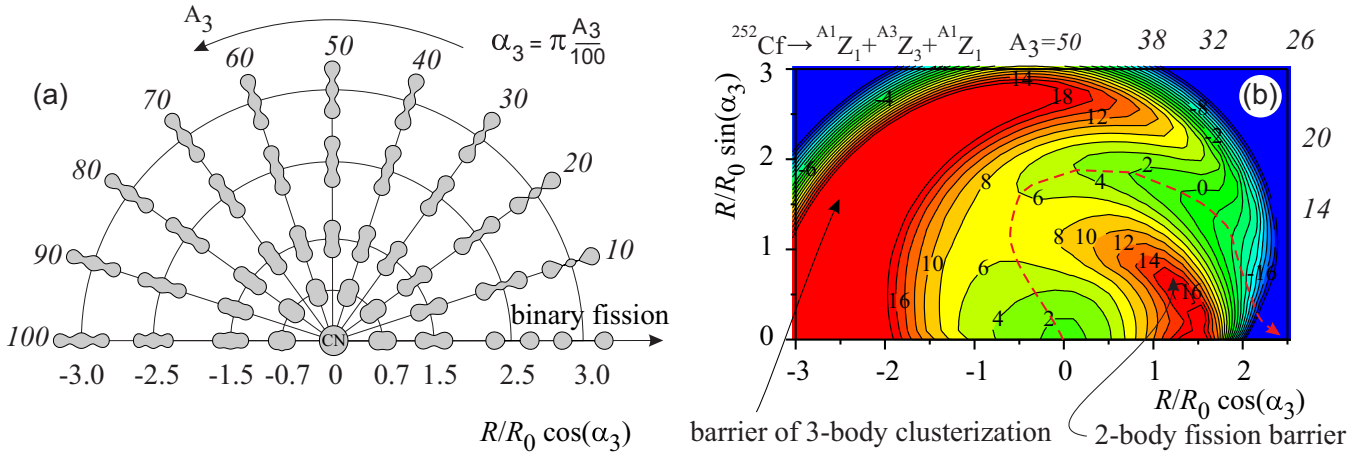

FIG. 2. Macroscopic part of the potential energy for fission of ^{252}Cf calculated for zero values of the deformation parameters (b) and nuclear shapes (a) depending on elongation and mass of third fragment (italic numbers). The contour lines are drawn over 2 MeV. The dashed curve shows one of possible binary fission paths.

using the corresponding relation for the ellipsoid nucleus. It is assumed in the calculations shown below that $\delta_U = 0$ and the neck parameter $\epsilon = 1$.

First, let us discuss the macroscopic (LDM) part of the potential energy. Figure 2 shows the LDM potentials for ^{252}Cf along with the corresponding nuclear shapes. The potential energy was calculated for the mirror-symmetric division of the nucleus ($A_1 = A_2$) for zero values of the deformation parameters ($\delta_i = 0$). For better visualization, the calculated potential energy is plotted as a function of $R/R_0 \cos(\alpha_3)$ and $R/R_0 \sin(\alpha_3)$, where $\alpha_3 = \pi A_3/100$ and R_0 is the radius of the spherical nucleus. One may see that the potential energy has two barriers. The first one, which is closer to the ground state, is the usual barrier of binary fission. The second one is the barrier of three-body clusterization, which prevents the system from the ternary fission. This barrier grows with the increase of the mass of the middle fragment. The origin of this effect is quite obvious—it is due to increase of the Coulomb forces. Such behavior of the second barrier has an important consequence that simple exchange of side and middle fragments alters the probability of the system decay. A larger probability of the ternary fission should be expected when the middle fragment has a smaller size (see below).

It should be stressed once more that the second barrier on the potential energy landscape has a purely macroscopic nature and its appearance is connected with the formation of the second neck in the nuclear shape on the way to the ternary fission. It is clear that the macroscopic structure of the potential landscape prevents actinides from the ternary decay. Large shell effects for the strongly deformed nuclear system are the only reason for observing a noticeable yield of ternary fission. Such shell effects in the actinide region can be expected for mass-asymmetric fission with the formation of a magic tinlike cluster as one of the fragments. In order to test the model on available experimental data [15], a few potential energy surfaces for ^{252}Cf have been calculated. The first one corresponds to the case when one of the outer fragments is ^{132}Sn. This potential energy along with the corresponding shell correction are shown in Fig. 3. The mass of the second (side) fragment is determined by the mass conservation $A_2 = 252 - 132 - A_3$. Three regions of strong shell effects are clearly seen. The first one leads to binary

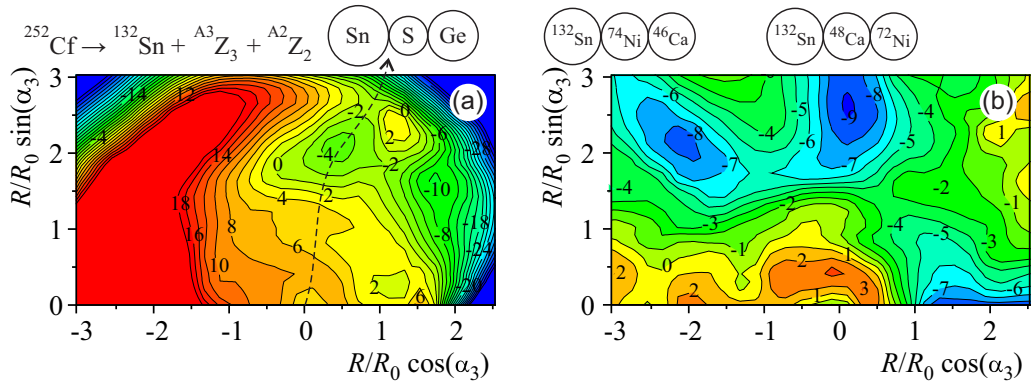

FIG. 3. Potential energy (a) and microscopic shell correction (b) for ternary fission of ^{252}Cf depending on elongation and mass of the third fragment calculated for zero value of the unified deformation. One of the side fragments is assumed to be ^{132}Sn. The dashed curve shows schematically the true ternary fission path.

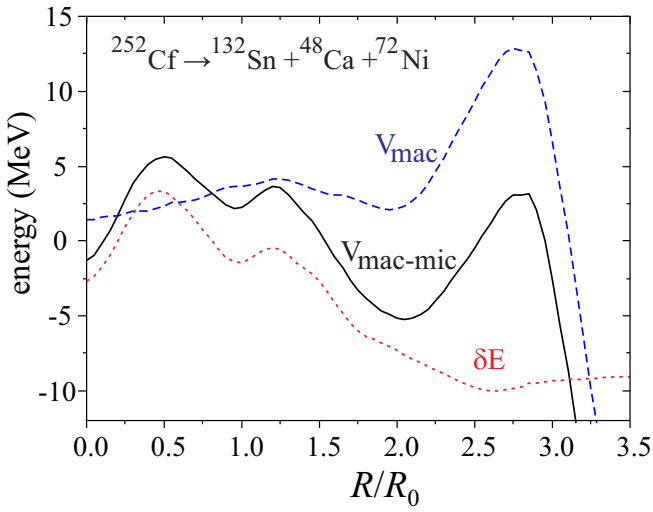

FIG. 4. Macroscopic potential energy (dashed line), shell correction (dotted line), and total macro-microscopical potential energy (solid line) of the ^{252}Cf nucleus corresponding to the ^{132}Sn+^{48}Ca+^{72}Ni ternary splitting.

fission with nearly symmetric "tin–cadmium" combination. Other two combinations correspond to the ternary fission with the formation of three magic clusters: tin, calcium, and nickel. The only difference between them is the order of fragments (small difference in the masses of calcium and nickel for these two combinations can be ignored). However, as discussed above, the probability of these two equal (in terms of fragment masses) combinations differs dramatically. One may see a rather well-pronounced valley on the potential energy surface corresponding to the formation of three fragments with the masses 132, 40, and 80 ("tin-sulfur-germanium" combination). This valley appears due to strong shell effects for the "tin-calcium-nickel" case. A small shift towards the smaller middle fragment (sulfur instead of calcium) is due to macroscopic properties of the ternary barrier. The ternary fission valley is quite well separated by the potential ridge from the binary fission valley. This means that the ternary fission of the ^{252}Cf nucleus into the "tin-sulfur-germanium" combination should be among the most probable true ternary fission channels of this nucleus. This result is in good agreement with the experimental data. The second found ternary combination, "tin-nickel-calcium," has negligible probability to be realized due to a large ternary fission barrier.

For better visualization of the potential energy structure discussed above, a cut of Fig. 3 along the ^{132}Sn+^{48}Ca+^{72}Ni ternary fission direction is shown in Fig. 4. In addition to the total potential $V_{\mathrm{mac-mic}}$, the microscopic shell correction δE and the macroscopic (LDM) part V_{mac} of the total potential are given. It is seen that the LDM potential makes the ternary fission nearly improbable due to large second (ternary fission) barrier while the first (binary fission) barrier is much lower. The shell effects substantially change the structure of the potential energy. First, the binary fission barrier becomes double-humped, which leads to the well-known phenomenon of spontaneous fission isomers. Second, the ternary fission barrier decreases drastically. It is important that the pocket in the potential energy between the binary and ternary fission barriers exists in both directions: elongation and mass asymmetry (see Fig. 3). This prevents the system trapped into the pocket from escape to the binary fission channel and, finally, increases the probability of the ternary fission process.

The increased ternary fission yield with the formation of ^{68,72}Ni was observed in Ref. [15]. The potential energy surfaces for these two cases are shown in Fig. 5. One may see again a well-separated ternary fission valley for the "nickel+calcium+tin" combination (the fragment masses are 72, 48, and 132). However, the potential energy surface calculated assuming ^{68}Ni as the first side fragment does not have a "good" ternary fission valley because of smaller absolute value of the shell correction that cannot "dig" a valley in the second (ternary fission) barrier. Both surfaces shown in Fig. 5 also have well-pronounced ternary fission valleys when the middle fragment has the mass around 16 (oxygen). This leads to the "nickel-oxygen-samarium" combination.

To conclude, the three-center shell model of deformed nucleus is developed in this paper. The model is an extension of the well-known two-center shell model and includes it as a special case. The three-center shell model is applied to analyze the general properties of the potential energy landscape on the example of the ternary fission of the ^{252}Cf nucleus. It was found that the ternary fission channel, being strongly suppressed by the macroscopic properties of the potential energy (additional barrier of ternary decay), may, however, be present with a

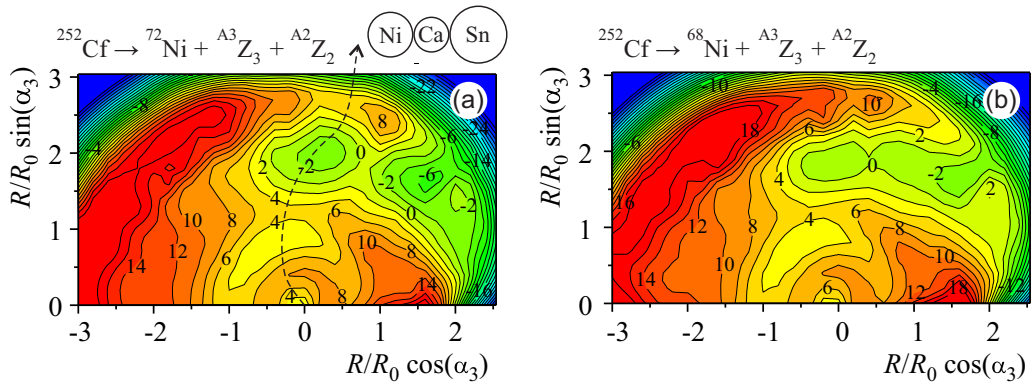

FIG. 5. The same as in Fig. 3(a) but with one of the side fragments assumed to be ^{72}Ni (a) and ^{68}Ni (b).

significant probability due to the shell effects. The potential energy has pronounced valleys favorable for true ternary fission with formation of doubly magic tin as one of the fragments and two other lighter (usually magic or semimagic) fragments. The positions of the found ternary fission fission valleys are in a good agreement with available experimental data.

ACKNOWLEDGMENTS

This work was supported in part by the RSA-JINR (Dubna) and ARE-JINR (Dubna) Cooperation program. I am grateful to Dr. A. Adel for interest in these studies and M. A. Naumenko for a careful reading of the manuscript.

[1] C. Wagemans, Ternary Fission in *The Nuclear Fission Process*, edited by Cyriel Wagemans (CRC Press, Boca Raton, FL, 1991), chap. 12.
[2] F. Gönnenwein, M. Wöstheinrich, M. Hesse, H. Faust, G. Fioni, and S. Oberstedt, in *Seminar on Fission*, edited by Cyriel Wagemans *et al.* (World Scientific, Singapore, 1999), p. 59.
[3] F. Gönnenwein, M. Mutterer and Yu. Kopatch, Europhys. News **36**, 11 (2005).
[4] G. M. Ter-Akopian *et al.*, Phys. At. Nucl. **67**, 1860 (2004).
[5] A. V. Ramaya *et al.*, Prog. Part. Nucl. Phys. **46**, 221 (2001).
[6] W. J. Swiatecki, *Second UN Int. Conf. on the Peaceful Uses of Atomic Energy, Geneva, Switzerland, 1958* (United Nations, Geneva, Switzerland, 1958), p. 651.
[7] H. Diehl and W. Greiner, Nucl. Phys. A **229**, 29 (1974).
[8] A. R. Degheidy and J. A. Maruhn, Z. Phys. A **290**, 205 (1979).
[9] R. A. Gherghescu and N. Carjan, J. Phys. G **36**, 025106 (2009).
[10] K. R. Vijayaraghavan, W. von Oertzen, and M. Balasubramaniam, Eur. Phys. J. A **48**, 27 (2012).
[11] K. R. Vijayaraghavan, M. Balasubramaniam, and W. von Oertzen, Phys. Rev. C **90**, 024601 (2014).
[12] W. von Oertzen, A. K. Nasirov, and R. B. Tashkhodjaev, Phys. Lett. B **746**, 223 (2015).
[13] M. L. Muga, C. R. Rice, and W. A. Sedlacek, Phys. Rev. Lett. **18**, 404 (1967).
[14] P. Schall, P. Heeg, M. Mutterer, and J. P. Theobald, Phys. Lett. B **191**, 339 (1987).
[15] D. V. Kamanin and Yu. V. Pyatkov, Lect. Notes Phys. **875**, 183 (2013).
[16] H. Schulheis and R. Schulheis, Phys. Lett. B **49**, 423 (1974).
[17] G. Royer, F. Haddad, and J. Mignen, J. Phys. G **18**, 2015 (1992).
[18] V. I. Zagrebaev, A. V. Karpov, and Walter Greiner, Phys. Rev. C **81**, 044608 (2010).
[19] P. Möller, J. R. Nix, W. D. Myers, and W. J. Swiatecki, At. Data Nucl. Data Tables **59**, 185 (1995).
[20] V. I. Zagrebaev, A. V. Karpov, Y. Aritomo, M. Naumenko, and W. Greiner, Phys. Part. Nuclei **38**, 469 (2007).
[21] V. M. Strutinsky, Nucl. Phys. A **95**, 420 (1967); **122**, 1 (1968).
[22] P. A. Cherdantsev and V. E. Marshalkin, Bull. Acad. Sci. USSR **30**, 341 (1966).
[23] P. Holzer, U. Mosel, and W. Greiner, Nucl. Phys. A **138**, 241 (1969).
[24] U. Mosel, J. Maruhn, and W. Greiner, Phys. Lett. B **34**, 587 (1971).
[25] J. Maruhn and W. Greiner, Z. Phys. A **251**, 431 (1972).
[26] W. D. Myers and W. J. Swiatecki, Nucl. Phys. A **601**, 141 (1996).
[27] P. Möller, A. J. Sierk, and A. Iwamoto, Phys. Rev. Lett. **92**, 072501 (2004).
[28] M. Abramowitz and I. A. Stegun, *Handbook of Mathematical Functions* (Dover, New York, 1965).